Construction and Building Materials 508 (2026) 145139

Contents lists available at ScienceDirect

Construction and Building Materials

journal homepage: www.elsevier.com/locate/conbuildmat

# Investigating the compressive and corrosion resistance properties of ultra-high-performance fiber-reinforced concrete enhanced with layered double hydroxide nanoparticles

Hakan Çağlar [b], Arzu Çağlar [a,*], Selcuk Çimen [d], Volkan Gönen [c]

[a] Faculty of Engineering and Architecture, Department of Architecture, Kırşehir Ahi Evran University, Kırşehir, Turkey
[b] Faculty of Engineering and Architecture, Department of Civil Engineering, Kırşehir Ahi Evran University, Kırşehir, Turkey
[c] Gönen Geomatics and Engineering, Kırşehir, Turkey
[d] Ministry of Interior, General Directorate of Security, Bayburt, Turkey

ARTICLE INFO

*Keywords:*
LDH Nanoparticles
Ultra-high-performance fiber-reinforced concrete (UHPFRC)
Chloride ingress
Sorptivity Measurements
Corrosive environment

ABSTRACT

Despite the growing interest in biodegradable layered double hydroxide (LDH) nanoparticles for cementitious materials, their influence on permeability-related transport behavior and chloride resistance of ultra-high-performance fiber-reinforced concrete (UHPFRC) has not yet been systematically investigated. In particular, the combined role of LDH nanoparticles and steel microfibers in governing moisture transport, chloride ingress, and mechanical performance of UHPFRC remains insufficiently understood. To address this research gap, the present study experimentally investigates the synergistic effects of LDH nanoparticles and steel microfibers on the compressive properties, permeability, and chloride resistance of UHPFRC. LDH nanoparticles were incorporated at dosages ranging from 0 to 2.5 wt% (0, 0.5, 1.0, 1.5, 2.0, and 2.5 wt%), while a constant steel microfiber content of 0.2 wt% was maintained. The performance of the modified concretes was evaluated through compressive strength tests, capillary water absorption and sorptivity measurements in accordance with ASTM C1585, mercury intrusion porosimetry (MIP) test and the rapid chloride migration test (RCMT). The results demonstrate that LDH nanoparticles effectively refine the cementitious matrix through pore refinement, hydration nucleation, and increased diffusion tortuosity, whereas steel microfibers primarily mitigate crack initiation and propagation, thereby limiting preferential transport pathways. A clear synergistic enhancement in mechanical and durability performance was observed, with a 22 % increase in compressive strength compared to the control mixture. Moreover, the incorporation of 2.0 wt% LDH resulted in approximately 37 % reduction in chloride migration and a pronounced decrease in capillary water absorption. At higher LDH contents, a reduction in efficiency was observed, indicating the existence of an optimal LDH dosage.

## 1. Introduction

Ultra-High-Performance Fiber-Reinforced Concrete (UHPFRC), an advanced cementitious composite characterized by its exceptional mechanical properties and durability characteristics, has garnered significant attention in a wide array of civil engineering applications, with particular emphasis on infrastructure projects and roadway pavements [1–3]. Its defining characteristics, such as ultra-high compressive strength, enhanced durability, and a dense, low-permeability microstructure, render it a highly suitable material for harsh roadway service conditions, where structures are subjected to heavy traffic loads, thermal cycling, and the ingress of corrosive agents [4]. Consequently, the deployment of UHPFRC in roadway pavements can significantly contribute to extending the service life of the infrastructure and minimizing the associated life-cycle costs of maintenance and rehabilitation. Particularly in aggressive exposure conditions, such as those found in coastal regions or areas subjected to de-icing salts, the strategic incorporation of advanced admixtures, like biodegradable nanoparticles, into the UHPFRC matrix holds the potential to further enhance its resilience against environmental deterioration mechanisms [5].

In recent years, extensive experimental research has focused on enhancing the durability and transport resistance of UHPFRC, particularly for applications in chloride-rich and aggressive service environments such as marine structures and bridge decks [6–8]. Owing to its

* Corresponding author.
*E-mail address:* arzu.caglar@ahievran.edu.tr (A. Çağlar).

https://doi.org/10.1016/j.conbuildmat.2026.145139
Received 12 August 2025; Received in revised form 31 December 2025; Accepted 5 January 2026
Available online 9 January 2026

dense microstructure and low water-to-binder ratio, UHPFRC exhibits inherently low permeability; nevertheless, chloride ingress remains a governing factor for long-term durability. Lv et al. [9] demonstrated that chloride transport in UHPFRC is primarily governed by pore connectivity and tortuosity rather than total porosity. Recent studies on concrete durability and failure mechanisms emphasize that long-term performance in aggressive environments is governed by the coupled effects of microstructural refinement, cracking behavior, and transport properties [10]. Investigations on corroded RC members and rehabilitated systems have shown that corrosion-induced damage and cyclic or combined loading significantly accelerate degradation by promoting crack-assisted transport pathways [11]. Research on precast concrete frames with replaceable or controllable plastic hinges further highlights the importance of local damage control in mitigating stiffness loss and durability deterioration [12,13]. At the material and interface level, advanced numerical, analytical, and data-driven studies demonstrate that bond degradation and interfacial damage between steel reinforcement and concrete strongly influence permeability and durability under both static and dynamic conditions [14].

High-fidelity mesoscale modeling approaches have been developed to accurately represent concrete heterogeneity and its impact on cracking and transport behavior, which is particularly relevant for dense materials such as UHPFRC [15]. In parallel, non-destructive and data-driven diagnostic techniques have been employed to identify internal damage that may correlate with enhanced chloride ingress [16]. Experimental and analytical investigations on UHPFRC structural elements under static, impact, and fatigue loading confirm that superior strength must be accompanied by effective control of cracking to ensure durability [17,18]. Moreover, recent advances in nonlocal modeling, constitutive algorithms, and dynamic material formulations provide robust tools for capturing damage evolution and environment-dependent responses in concrete materials [19–22]. Sustainability-driven studies on low-shrinkage binders, carbonation, and low-carbon composite systems further underline the critical role of microcracking and transport resistance in long-term durability, especially in chloride-prone environments [23,24]. Collectively, these studies indicate that durability is inherently multi-scale, motivating the present investigation into nano-scale matrix modification and fiber-based crack control in UHPFRC.

The use of nanoparticles has attracted significant attention across various engineering disciplines [25–28], particularly in concrete technology, due to their unique physicochemical properties, high specific surface area, and ability to effectively tailor microstructural and durability-related characteristics [29]. Recent experimental studies provide a clear rationale for adopting low nanoparticle replacement ranges (sub-percent to ~2 wt% of cement/binder) in dense, low-w/b systems such as UHPFRC: the performance gains are typically governed by (i) pore refinement and nucleation/packing effects at low dosages and (ii) loss of efficiency at higher dosages due to dispersion instability and the formation of weak zones. For example, Bao et al. [30] quantified chloride ingress using field exposure in real marine tidal/splash zones for up to 720 days and showed how transport parameters (e.g., diffusion coefficient and surface chloride) strongly depend on mixture design and exposure conditions—highlighting the need to evaluate chloride resistance with targeted, durability-oriented experiments rather than only strength tests. In UHPFRC-class materials, Saladi et al. [31] demonstrated that rapid chloride migration (NT BUILD 492) meaningfully differentiates UHPFRC penetrability levels (with non-steady-state migration coefficients in the $\sim 10^{-13}$ $m^2/s$ order for several UHPFRC), underscoring why small binder-level modifications can be detectable in standardized transport testing. Complementarily, Saleh et al. [32] experimentally examined SWSS- UHPFRC with varying SCM proportions and reported coupled changes in mechanical response, transport indicators, and chloride binding—supporting the practice of selecting a narrow nanoparticle window to avoid workability/dispersion penalties while still targeting measurable durability gains. Within this experimental context, recent UHPFRC literature also shows that nano-additives are commonly investigated in the 0.5–2.0 wt% band because this range is large enough to modify hydration/packing yet small enough to remain practically dispersible.

Recent studies have highlighted that the durability and failure behavior of UHPFRC are governed by a complex interplay between microstructural densification, cracking mechanisms, and transport properties. Li et al. [33] demonstrated that although amorphous silica can significantly enhance the fracture resistance of UHPFRC through matrix densification, excessive shrinkage-induced microcracking may counteract these benefits, emphasizing the importance of microstructural stability for long-term durability. Similarly, Li et al. [34] reported that optimizing aggregate characteristics can markedly improve the mixed-mode cracking resistance of UHPFRC by enhancing crack deflection and energy dissipation capacity. From a durability perspective, Gu et al. [35] employed a multi-scale modeling framework to show that chloride diffusivity in UHPFRC is strongly dependent on pore connectivity and microstructural refinement, rather than solely on total porosity. Moreover, a recent review by Ojaghi et al. [36] emphasized that nanoparticle additives can play a critical role in improving fiber–matrix adhesion and mitigating degradation in corrosive traffic environments, although their influence on transport-related durability parameters of UHPFRC remains insufficiently explored. These studies collectively indicate that while significant progress has been made in understanding fracture and durability mechanisms of UHPFRC, the role of emerging nanomaterials in simultaneously controlling permeability, cracking behavior, and chloride resistance requires further systematic investigation, providing a clear motivation for the present work.

Hendrix et al. [37] confirmed—through fresh/rheology indicators, compressive strength, pore structure metrics, and single-fiber pull-out tests—that the benefit of nanosilica is conditional on dispersion stability, and that poorly stabilized systems can negate expected gains, which mechanistically supports using conservative dosage steps rather than aggressive replacement levels. For LDH-type additives specifically, Zhou et al. [38] reported that adding calcined hydrotalcite (LDH family) alters chloride penetration behavior, with an optimum appearing at lower contents, consistent with the general “optimum-then-decline” pattern seen for nanofillers. More broadly, durability studies in seawater/marine exposure (e.g., PLC-based UHPFRC in seawater for long durations; UHPFRC with coarse aggregate optimizing resistance to chloride penetration) emphasize that chloride resistance is highly sensitive to microstructure and ITZ quality—properties that nanomodification targets most effectively at low dosages [39–41]. Finally, emerging LDH-based systems tested under marine environments also adopt modest contents and focus on pore structure, hydration, and durability indicators, aligning with the same dosage philosophy [42–45].

Recent studies have increasingly focused on the application of LDHs as functional micro- and nano-additives in cementitious composites to enhance mechanical performance and durability-related properties. Ramazani et al. [46] experimentally and numerically investigated the flexural behavior of lightweight steel fiber reinforced concrete incorporating biodegradable LDH microparticles. Their results demonstrated a substantial improvement in flexural strength and toughness at low LDH contents, with an optimal dosage close to 1 wt% in fiber-free mixtures. However, when the LDH content was increased to 2 wt%, a reduction in load-bearing capacity was observed, which was attributed to particle agglomeration and matrix heterogeneity. This study highlighted that LDH effectiveness is strongly dosage-dependent and that excessive contents may negate the beneficial filler and nucleation effects. Similarly, Mohsen et al. [47] examined the influence of Zn–Al–$CO_3$ LDH nanoparticles on alkali-activated slag pastes and reported that low LDH dosages (0.5–1.0 wt%) significantly enhanced compressive strength and microstructural compactness, while maintaining acceptable setting times. Their findings emphasized that LDHs can effectively improve cementitious matrices within a limited dosage window, beyond which adverse rheological and hydration-related effects may occur.

More recently, Yu et al. [48] studied the role of highly dispersed LDH nano-platelets on chloride binding and corrosion protection in cementitious materials. Their work demonstrated that LDHs improve chloride resistance primarily through ion-exchange mechanisms and microstructural refinement, while also revealing that agglomeration at higher dosages limits pore refinement efficiency. These observations further confirm the existence of an optimal LDH content for durability enhancement. Pang et al. [49] developed highly dispersed polycarboxylate-modified LDH nanoparticles and demonstrated that their stable dispersion and high surface reactivity significantly accelerated cement hydration by acting as effective nucleation sites. Their results confirmed that low dosages of well-dispersed LDH can markedly enhance early-age compressive strength and hydration kinetics without compromising matrix stability.

In the context of ultra-high-strength and fiber-reinforced concretes, Kalateh et al. [50] conducted an experimental–numerical investigation on the pull-out behavior of steel fibers embedded in UHSC modified with biodegradable LDH nanoparticles. They reported that an LDH content of approximately 2 wt% maximized fiber–matrix bond strength and pull-out resistance, whereas higher dosages led to strength reduction due to agglomeration-induced weak zones. Their findings indicate that LDH contents up to about 2 wt% are effective in improving both matrix properties and fiber–matrix interaction. Consistent trends were also reported by Qu et al. [51], who investigated the relationship between LDH particle size, dosage, and chloride transport in cement mortars. Their results showed that increasing LDH content reduced chloride migration coefficients due to enhanced tortuosity and chloride binding; however, the marginal improvement in mechanical properties diminished when the dosage increased from 1 wt% to 2 wt%, again attributed to nano-particle agglomeration. Collectively, these studies establish that LDH additions in cementitious systems are most effective within a low-dosage range, typically not exceeding approximately 2 wt% of cement. Other nanomaterials, such as nano-calcium carbonate (nano-$CaCO_3$) and nano-silica (nano-$SiO_2$), have also demonstrated improvements in the strength and toughness of UHPFRC [52–54]. Long-term studies, with durations of up to 365 days, have confirmed the efficacy of nano-metakaolin in reducing chloride penetration depth and enhancing the overall durability of UHPFRC [55,56]. Collectively, these findings indicate that nanomaterials, particularly advanced nano-clays like nano-metakaolin, can substantially augment the resilience of UHPFRC against chloride-induced deterioration. Building upon these advances, the present study investigates the role of LDH nanoparticles as a cement replacement in UHPFRC, with particular emphasis on mechanical performance and chloride-related durability.

To the best of the authors' knowledge, the effects of LDH nanoparticles on the corrosion-related durability and permeability characteristics of UHPFRC have not yet been systematically investigated. The intrinsic advantages of this material, including its ultra-high compressive strength, superior durability, and low permeability, render it a highly suitable candidate for pavement structures, particularly under severe environmental conditions. The integration of UHPFRC with steel fibers and other advanced admixtures has been shown to significantly enhance the mechanical properties and long-term durability of these pavements. Building upon this foundation, the present study aims to investigate the influence of biodegradable LDH nanoparticles on the mechanical behavior, permeability, and chloride ingress resistance of UHPFRC subjected to a corrosive marine environment. In this framework, LDH nanoparticles predominantly modify the matrix microstructure and ion-transport behavior, whereas steel microfibers act at the crack scale; their interaction yields a coupled mechanism that simultaneously suppresses matrix permeability and crack-assisted chloride ingress. This investigation was conducted by incorporating LDH nanoparticles as a partial cement replacement at dosages of 0–2.5 wt%, alongside a 0.2 % volume fraction of steel microfibers, to systematically evaluate their combined effect on concrete properties. The findings of this research are anticipated to provide a scientific basis for the design and optimization of UHPFRC mixtures for infrastructure projects under comparable exposure conditions. Furthermore, the application of LDH nanoparticles as a functional admixture in UHPFRC is posited as a sustainable and effective strategy for improving the durability and performance of roadway infrastructure.

## 2. Materials and methods

This section details the experimental methodology employed to assess the mechanical properties and durability performance of UHPFRC modified with biodegradable LDH nanoparticles. The investigation encompasses an evaluation of key durability indicators, including chloride ion migration and permeability characteristics.

### 2.1. Characteristics of steel fibers

Steel fibers were incorporated into the UHPFRC mixtures as reinforcement to enhance the material's mechanical properties and durability. In this investigation, a constant volume fraction of 0.2 % steel fibers was utilized across all concrete mixtures. The primary geometric and mechanical properties of these fibers are summarized in Table 1. A visual representation of the fibers is provided in Fig. 1. Furthermore, the influence of the steel fiber inclusion on the compressive strength of the concrete was systematically evaluated.

### 2.2. Biodegradable LDH nanoparticles

In this study, LDH nanoparticles were utilized as a supplementary cementitious material in the UHPFRC mixtures. These nanoparticles were selected due to their biodegradable nature and their demonstrated potential to enhance the mechanical properties and durability of concrete, particularly its resistance to chloride ion ingress. The key physicochemical characteristics of the LDH nanoparticles, including their particle size, morphology, and structural features, are presented in this section.

SEM observations (Fig. 2) reveal that the LDH nanoparticles possess nanoscale platelet-like morphologies with particle sizes on the order of several tens of nanometers. Their high surface area and layered structure promote strong interactions with the cementitious matrix, facilitating microstructural refinement and enhanced resistance to chloride ingress. From a morphological standpoint, LDH nanoparticles are characterized by a layered platelet-like structure, which distinguishes them from conventional particulate fillers. This lamellar configuration provides a high density of reactive surfaces and interlayer sites, endowing the nanoparticles with notable ion-exchange capability and chemical activity. Such features are particularly beneficial in cement-based systems, where LDH nanoparticles can contribute to microstructural refinement, enhanced binding of aggressive ions, and improved resistance against chloride penetration. The main characteristics of the LDH nanoparticles are summarized in Table 2.

### 2.3. UHPFRC mix design

The mix proportions for the UHPFRC were formulated based on the weight and volume fractions of the constituent materials, including

**Table 1**
Geometric and mechanical properties of the steel fibers.

| Property | Value |
|---|---|
| Diameter (mm) | 0.5 |
| Length (mm) | 15 |
| Aspect ratio [$l/d$] | 0.3 |
| $f_y$ (MPa) | 230 |
| $f_u$ (MPa) | 450 |
| $E$ (GPa) | 205 |


**Fig. 1.** The brass-coated steel microfibers employed in this study.

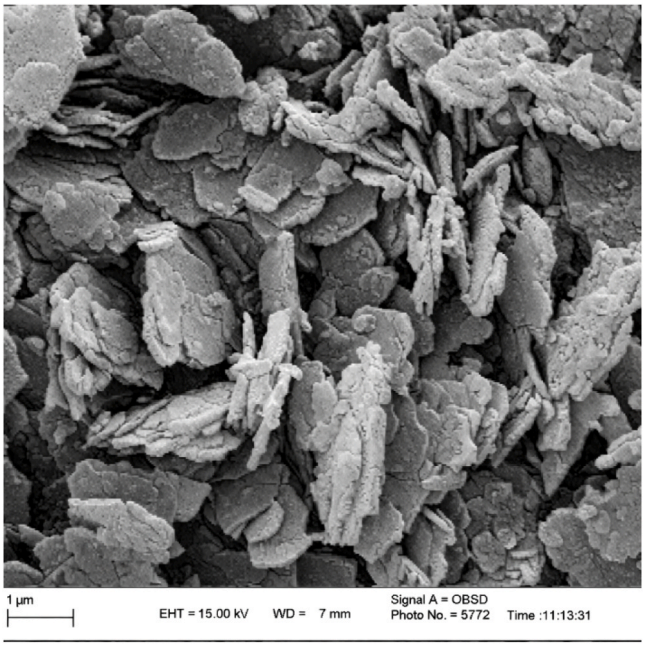


**Fig. 2.** Scanning electron microscopy (SEM) micrograph of the LDH nanoparticles.

**Table 2**
Summary of the properties and characteristics of the layered double hydroxide (LDH) nanoparticles.

| Property | LDH Nanoparticle Characteristics |
|---|---|
| Particle size | 20–100 nm |
| Shape | Sheet-like or layered |
| Structure | Layered structure with alternating positive and negative layers |
| Type of adsorbed ions | Calcium, magnesium, aluminum ions, and other mineral ions |
| Specific surface area | High surface area leading to increased adhesion and reactivity |
| Chemical properties | Ability to adsorb and retain ions, high ion-exchange capacity |
| Biodegradability | Biodegradable and suitable for use in sustainable concretes |
| Applications | Improved mechanical properties, chloride penetration resistance, enhanced concrete durability |
| Effect on concrete | Increased compressive strength, reduced permeability, enhanced durability against corrosive conditions |

Portland cement, water, LDH nanoparticles, and steel fibers. In this investigation, five distinct mix designs were developed. These mixtures incorporated LDH nanoparticles as a partial cement replacement at five different dosages: 0 % (control), 0.5, 1.0, 1.5, 2.0 and 2.5 by weight of cement (wt%). The selected LDH replacement levels (0, 0.5, 1.0, 1.5, and 2.0 wt% of cement) were determined based on recent experimental studies on UHPFRC and high-performance cementitious composites, which indicate that the effectiveness of nano- and micro-scale mineral additives is generally confined to low dosage ranges [46,47]. Previous investigations have shown that LDH-type and other mineral nano-additives significantly improve pore refinement, hydration kinetics, and chloride transport resistance when used at contents below approximately 2 wt% of cement, whereas higher dosages tend to promote particle agglomeration and matrix heterogeneity, leading to diminishing performance gains [48,50]. Accordingly, 2 wt% was adopted as a rational upper bound in this study, while a step size of 0.5 wt% was selected to capture dose–response trends and identify a potential optimum LDH content without introducing excessive experimental variability.

Steel microfibers were incorporated at a constant dosage of 0.2 wt% of cement, corresponding to a fixed mass of 150 g in each mixture. It should be noted that the steel microfiber content was intentionally maintained at a constant volume fraction throughout all mixtures. The selected dosage corresponds to a commonly reported optimum range for UHPFRC, which ensures effective crack-bridging capacity, strain-hardening behavior, and stable post-cracking performance. The primary objective of the present experimental program was not to re-evaluate the influence of fiber dosage—an aspect extensively addressed in previous UHPFRC studies—but rather to isolate and quantify the role of LDH nanoparticles as a cement-replacement additive on mechanical properties and durability-related transport characteristics. By fixing the steel microfiber content, potential interaction effects between fiber volume fraction and nanoparticle dosage were minimized, allowing the observed variations in permeability, chloride resistance, and strength to be predominantly attributed to the incorporation of LDH.

The water-to-binder ratio (w/b = 0.185) reported in Table 3 corresponds to the nominal design mixing water, which was intentionally kept constant across all mixtures to enable an unbiased comparison of LDH dosage effects. The potential water uptake of LDH particles was considered by adopting a dispersion-controlled mixing protocol (LDH introduced into the liquid phase under high-shear mixing) and by monitoring fresh-state consistency during mixing. Within the investigated low replacement levels (≤2.0 wt% of cement), the absolute LDH mass is small relative to the total binder and mixing water; thus, any LDH-associated water sequestration is expected to be minor and did not cause observable abnormal stiffening under the adopted procedure. It is noted that for substantially higher LDH contents, explicit water-demand correction or pre-wetting/dispersion calibration may become necessary.

The UHPFRC was produced using a combination of materials, including Portland cement, fine sand, silica fume, quartz powder, a high-range water reducer (superplasticizer), steel fibers, and the biodegradable LDH nanoparticles. Portland cement served as the primary binding agent, while fine sand and quartz powder contributed to the refinement of the granular skeleton and the overall strength of the matrix. Silica fume, a highly reactive pozzolanic admixture, was incorporated to enhance the concrete's strength and its resistance to chemical ingress. The superplasticizer was employed to achieve adequate workability at a low water content. Steel fibers were added to improve the tensile strength and control cracking. Finally, the LDH nanoparticles, acting as a partial cement replacement, were introduced to augment the mechanical properties and enhance the concrete's resistance to chloride attack and other corrosive agents, thereby promoting its long-term stability and durability in aggressive environments. The detailed proportions for the different UHPFRC mixtures are presented in Table 3.

### *2.4. Determination of Mechanical Properties of LDH-Modified UHPFRC*

This subsection outlines the experimental tests conducted to determine the mechanical properties of the UHPFRC modified with LDH

**Table 3**
Mix proportions of UHPFRC with varying dosages of LDH nanoparticles.

| LDHs Nanoparticles Percentage (wt%) | Cement (g) | LDHs Nanoparticles (g) | Fine Sand (g) | Silica Fume (g) | Quartz Powder (g) | Superplasticizer (g) | Steel Fibers (g) | Water-to-Cement Ratio |
|---|---|---|---|---|---|---|---|---|
| 0 % (Control Mix) | 695 | 0 | 992 | 228 | 206 | 60 | 150 | 0.185 |
| 0.5 % | 692.3 | 3.5 | 992 | 228 | 206 | 60 | 150 | 0.185 |
| 1.0 % | 689 | 6.9 | 992 | 228 | 206 | 60 | 150 | 0.185 |
| 1.5 % | 685.7 | 10.4 | 992 | 228 | 206 | 60 | 150 | 0.185 |
| 2.0 % | 681.1 | 13.9 | 992 | 228 | 206 | 60 | 150 | 0.185 |
| 2.5 % | 677.6 | 17.4 | 992 | 228 | 206 | 60 | 150 | 0.185 |

nanoparticles. Specifically, the compressive strength test was performed to evaluate the influence of LDH nanoparticles on the strength development of the concrete. Specimens from the different mixtures were subjected to testing at various curing ages, namely 7, 28, and 90 days.

The compressive strength of the UHPFRC mixtures was evaluated using a SANTAM universal testing machine with a 10-kN load capacity. Cubic specimens with dimensions of 50 × 50 × 50 mm were cast for this purpose. After curing for 28 days under controlled laboratory conditions (temperature of 22 ± 2 °C and relative humidity of approximately 90 %), the specimens were tested under uniaxial compression. The loading was applied in displacement-controlled mode at a constant rate of 0.2 mm/min, following the procedures outlined in ASTM C109/C109M. During the test, the applied load was continuously monitored until complete failure of the specimen occurred. The maximum recorded load was subsequently used to calculate the compressive strength. The obtained results were employed to assess the influence of LDH nanoparticle incorporation on the compressive performance and mechanical efficiency of the UHPFRC mixtures.

### 2.5. Rapid Chloride Migration Test (RCMT)

The rapid chloride migration test (RCMT) is a standardized method for assessing the resistance of concrete to chloride ion ingress. This test is particularly relevant for evaluating the durability of concrete in aggressive environments, such as marine zones and roadways subjected to de-icing salts. In the present study, the RCMT was conducted to investigate the effect of LDH nanoparticles on the chloride resistance of UHPFRC. By accelerating the migration of chloride ions into the concrete specimens, this test provides crucial data on the material's ability to withstand corrosive agents.

For this test, 50 × 50 × 50 mm cubic specimens were prepared from each of the different mix designs. Following a 28-day curing period under standard laboratory conditions (22 ± 2°C and 95 % relative humidity), the specimens were conditioned and then subjected to the test protocol. The cathode cell was filled with a 10 % sodium chloride (NaCl) solution, which served as the source of chloride ions, while the anode cell was filled with a sodium hydroxide (NaOH) solution. An external electrical potential was applied across the specimen using an ElectroChloride-500 apparatus to accelerate the migration of chloride ions into the concrete. This potential was maintained for a duration of 24 h. The specimen preparation and setup in the aggressive exposure environment are illustrated in Fig. 3. This standardized test is essential for evaluating the chloride resistance of concrete, particularly for high-durability concrete structures intended for severe service environments. The results obtained from the RCMT allow for a direct assessment of the efficacy of LDH nanoparticles in reducing the chloride permeability of UHPFRC and thereby enhancing its overall durability against corrosive agents.

### 2.6. Capillary water absorption

The capillary water absorption behavior of the LDH-modified UHPFRC mixtures was evaluated following the procedure specified in ASTM C1585 [57]. Cubic specimens with a side length of 50 mm were used for this purpose. Prior to testing, the specimens were dried in an oven at 100 ± 15 °C for 24 h until a constant mass was attained. After drying, all lateral faces and the top surface of each specimen were carefully sealed with aluminum tape and a nylon-based coating to prevent lateral moisture ingress. This sealing configuration ensured that water penetration occurred exclusively through the bottom surface, thereby establishing a one-dimensional capillary absorption condition, as schematically illustrated in Fig. 4.


**Fig. 3.** Specimen preparation and setup for exposure to the aggressive environment.

After sealing, each specimen was weighed to determine its initial dry mass. The specimens were then positioned in a water-filled container, ensuring that the water level was maintained at approximately 3 mm above the bottom surface of the cube, as illustrated in Fig. 4. During the test, the mass gain of each specimen was measured at predefined intervals to monitor capillary water uptake. Measurements were taken at 1–60 min, followed by 2–6, and 24 h, and subsequently at 2–8 days from the start of exposure. Based on the difference between the recorded mass at each interval and the initial dry mass, the initial and secondary water absorption rates were calculated in accordance with the procedures outlined in ASTM C1585.

Capillary water absorption tests were conducted in accordance with ASTM C1585 to evaluate the capillary-driven moisture transport behavior of UHPFRC mixtures. Prior to testing, specimens were dried to a constant mass and then exposed to water through one surface, while all other surfaces were sealed to ensure one-dimensional water ingress. The increase in specimen mass due to water absorption was recorded at predefined time intervals.

The cumulative water absorption per unit exposed surface area, $I(t)$, was calculated using the following expression:

$$I(t) = \frac{\Delta m(t)}{A} \tag{1}$$

where $\Delta m(t)$ is the increase in specimen mass at time $t$ (kg), and $A$ is the area of the surface exposed to water ($m^2$). The cumulative absorption is expressed in units of $kg{\cdot}m^{-2}$.

Sorptivity (S), defined as the slope of the linear relationship between

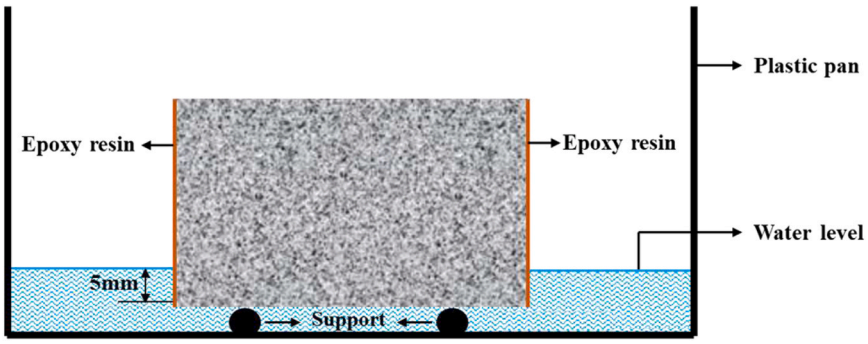


**Fig. 4.** A schematic diagram illustrating the specimen setup for the capillary water absorption test, in accordance with ASTM C1585 [58].

cumulative capillary water absorption and the square root of time during the initial absorption stage, is a fundamental parameter for evaluating the rate of capillary-driven moisture ingress in cementitious materials. Sorptivity, $S$, was determined from the linear relationship between cumulative water absorption and the square root of time, as defined by ASTM C1585:

$$I(t) = b + S\sqrt{t} \tag{2}$$

where $t$ is time (s), $S$ is the sorptivity ($kg{\cdot}m^{-2}{\cdot}s^{-1/2}$), and $b$ is a constant accounting for surface effects at the initial contact with water. The sorptivity value was obtained as the slope of the best-fit linear regression of I(t) versus $t^{1/2}$ over the initial absorption period.

Lower values of sorptivity indicate reduced capillary pore connectivity and improved resistance to water ingress. The calculated sorptivity values were subsequently used to quantitatively compare the capillary transport performance of UHPFRC mixtures with different LDH nanoparticle contents.

The chloride migration coefficient (CMC) is a key durability parameter that quantifies the resistance of cementitious materials to chloride ion transport under an applied electrical field. It is commonly determined using the RCMT and represents the effective rate at which chloride ions penetrate the concrete matrix. Lower values of CMC indicate reduced chloride permeability and enhanced resistance against chloride-induced corrosion of steel reinforcement. The equation assumes a steady-state condition, where the chloride ion flux is proportional to the concentration gradient across the concrete surface. The chloride migration coefficient was determined using the Rapid Chloride Migration Test (RCMT) following NT BUILD 492 as [59]:

$$CMC = \frac{0.0239 \times (273+T) \times L}{(U-2) \times t} \times \left( x_d - 0.0238\sqrt{\frac{(273+T) \times L \times x_d}{(U-2)}} \right) \tag{3}$$

where $T$ denotes the mean of the initial and final absolute temperatures of the analyte (∘C); $U$ stands for the electrical potential difference ($V$); $t$ represents the exposure time ($h$); $x_d$ signifies the average value of the penetration depth (mm); and $L$ indicates the thickness of the specimen (mm).

### 2.7. Mercury Intrusion Porosimetry (MIP) Test

Mercury Intrusion Porosimetry (MIP) was employed to quantitatively characterize the pore structure and pore size distribution of UHPFRC specimens incorporating different LDH contents. The test was conducted to evaluate the influence of LDH dosage on total porosity, capillary pore refinement, and pore connectivity, which are directly related to capillary water absorption and durability performance. Prior to testing, UHPFRC specimens were sectioned into small fragments with characteristic dimensions of approximately 5–8 mm to ensure representative pore structure while minimizing structural damage. The samples were subsequently solvent-exchanged using isopropanol to arrest ongoing hydration reactions and prevent microstructural alteration. After solvent exchange, the specimens were dried under vacuum at low temperature (≤50 °C) until a constant mass was achieved, thereby avoiding thermal damage or pore collapse.

MIP measurements were performed using an automated mercury intrusion porosimeter, capable of applying intrusion pressures ranging from low vacuum conditions to a maximum pressure of approximately 400 MPa. This pressure range corresponds to the measurable pore diameter range from approximately 100 μm down to about 5 nm, calculated based on the Washburn equation. The surface tension of mercury was taken as 0.485 N/m, and the contact angle between mercury and the cementitious material was assumed to be 140°, in accordance with commonly accepted values reported for cement-based composites.

The test procedure and data interpretation followed the principles outlined in ASTM D4404 and ASTM D4284, as well as widely adopted protocols in cementitious materials research. The cumulative intrusion volume, differential pore size distribution, total porosity, and critical pore diameter were obtained from the intrusion curves. Particular attention was paid to the capillary pore range (typically 10–1000 nm), which governs capillary water absorption and transport behavior in UHPFRC.

For each mixture, at least two representative specimens were tested to ensure repeatability. The reported results correspond to the average values obtained from repeated measurements. The MIP data were subsequently correlated with capillary water absorption results and compressive strength measurements to elucidate the role of LDH nanoparticles in modifying the pore structure and transport properties of UHPFRC.

## 3. Results and discussion

This section presents and discusses the results obtained from the experimental program conducted on the LDH-modified UHPFRC. The analysis focuses on the material's mechanical performance, durability characteristics, and resistance to chloride-induced degradation, with a systematic evaluation of the influence of LDH nanoparticles.

### 3.1. Compressive strength under normal and chloride-exposed conditions

Fig. 5 presents the compressive strength performance of UHPFRC mixtures containing different LDH nanoparticle contents. The results include specimens evaluated after 28 days of curing under standard conditions, as well as specimens tested at 90 days under both normal curing and chloride-exposed environments. This comparison enables assessment of the combined effects of LDH dosage, curing age, and environmental exposure on the compressive behavior of UHPFRC. The mean 28-day compressive strength of the control specimen (0 % LDH) was recorded as 148.5 MPa, establishing a baseline for comparison. The

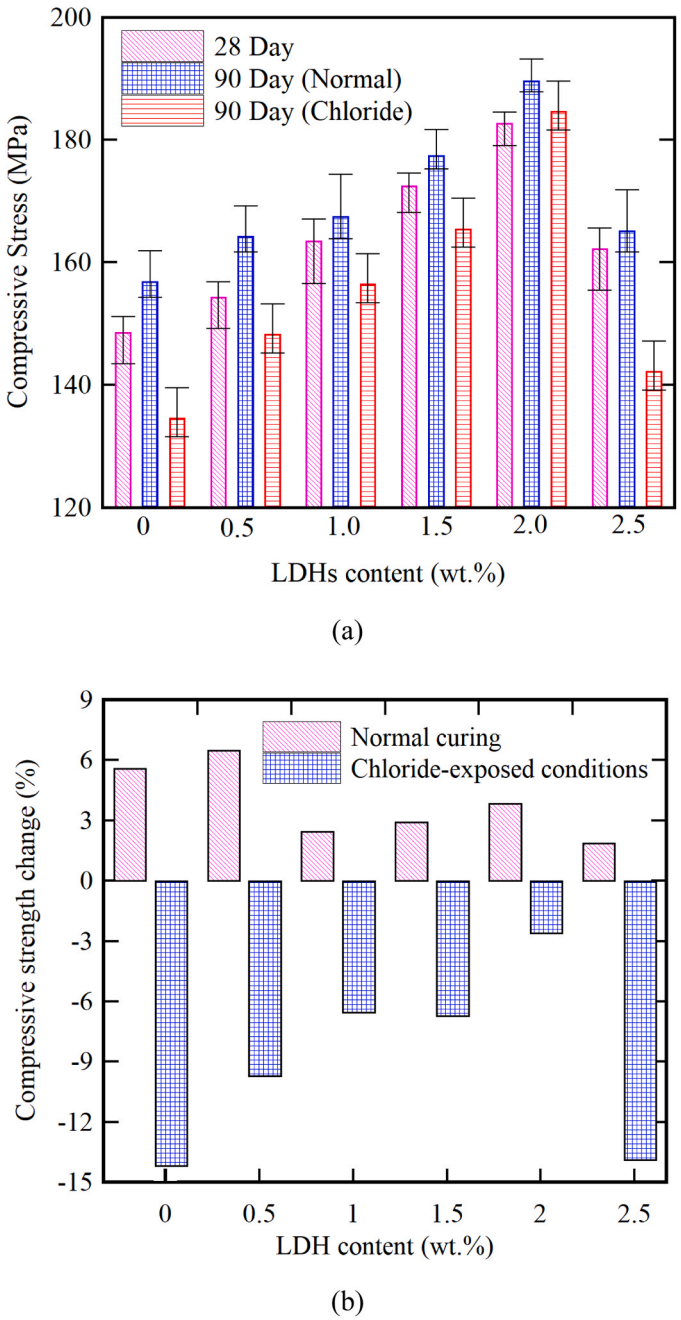


**Fig. 5.** (a) Compressive strength of UHPFRC mixtures with varying LDH nanoparticle dosages, (b) Percentage change in compressive strength of UHPFRC at 90 days relative to 28 days under normal curing and chloride-exposed conditions as a function of LDH content.

results reveal a pronounced positive effect of LDH nanoparticle incorporation on the mechanical performance of the UHPFRC. A clear trend of increasing compressive strength was observed as the LDH content was raised from 0 % to 2.0 %. Specifically, the mixture containing 2.0 % LDH nanoparticles achieved a 28-day compressive strength of 182.67 MPa, representing a significant enhancement of 21.95 % relative to the control specimen. This strength enhancement can be attributed to several microstructural improvements. The nanoparticles act as a filler, physically occupying interstitial voids within the matrix, which leads to a denser, more compact microstructure and improved inter-particle bonding. Furthermore, LDH nanoparticles can serve as nucleation sites, promoting the formation of additional hydration products and thereby enhancing the overall cohesion and intrinsic strength of the cementitious matrix.

Conversely, a decline in compressive strength was observed at dosages exceeding the optimum level, as exemplified by the 2.5 % LDH mixture. Although this mixture still exhibited a 9.67 % strength increase over the control (achieving a mean strength of 162.87 MPa), its performance was notably inferior to that of the 2.0 % LDH mixture. This trend suggests that an excessive concentration of nanoparticles may lead to agglomeration. Such agglomerates can introduce microscopic voids and disrupt the homogeneity of the matrix, thereby impairing the bond between the cementitious phases and aggregates and ultimately reducing the composite's overall strength. From a materials science perspective, these findings underscore that the incorporation of nanomaterials must be carefully optimized within a specific range. Consequently, the results of this investigation clearly identify a 2.0 % dosage of LDH nanoparticles as the optimum content for maximizing the mechanical performance of the UHPFRC developed in this study. Any further increase beyond this threshold is likely to induce detrimental effects on the microstructure, leading to a degradation in performance. This conclusion holds significant implications for the design and proportioning of high-strength, high-durability concrete mixtures for advanced infrastructure projects.

Fig. 5b illustrates the percentage change in compressive strength from 28 to 90 days. While all mixtures exhibited strength gain under normal curing, specimens exposed to the chloride environment showed a reduced growth rate. Notably, LDH-modified mixtures demonstrated a mitigated strength reduction, indicating that LDH incorporation enhances long-term strength stability under aggressive exposure. A quantitative comparison reveals that all mixtures exhibit strength gain from 28 to 90 days under normal curing, indicating continued hydration and matrix densification. Specifically, the 90-day compressive strength under normal conditions increased by approximately 5.5 % (0 wt%), 6.5 % (0.5 wt%), 2.4 % (1.0 wt%), 2.9 % (1.5 wt%), 3.8 % (2.0 wt%), and 1.9 % (2.5 wt%) relative to the corresponding 28-day values. This confirms that LDH incorporation does not hinder long-term strength development within the investigated dosage range. In contrast, exposure to the chloride environment resulted in a systematic reduction in compressive strength compared with specimens cured under normal conditions. For the control mixture (0 wt% LDH), the 90-day compressive strength decreased by approximately 14.1 % relative to the 90-day normal-cured specimen. Notably, the incorporation of LDH nanoparticles significantly mitigated this strength loss. At LDH contents of 0.5, 1.0, 1.5, and 2.0 wt%, the corresponding reductions were limited to approximately 9.8 %, 6.6 %, 6.7 %, and 2.6 %, respectively, indicating a pronounced improvement in resistance to chloride-induced degradation. The mixture containing 2.0 wt% LDH exhibited the lowest strength reduction, suggesting an optimal balance between matrix densification and durability enhancement. However, further increasing the LDH content to 2.5 wt% led to a renewed increase in strength loss under chloride exposure, reaching approximately 13.9 %, comparable to the control mixture. At 2.5 wt% LDH, the reduction in performance is attributed to nanoparticle agglomeration in the very low w/b UHPFRC matrix. Excess LDH promotes cluster formation, creating microstructural heterogeneities and weak zones that diminish the filler/nucleation benefits and may locally increase transport connectivity, which becomes more detrimental under chloride exposure. This behavior quantitatively supports the presence of an optimum LDH dosage, beyond which particle agglomeration and local matrix heterogeneity may offset the beneficial effects of pore refinement and chloride transport inhibition.

Overall, the quantitative results demonstrate that LDH nanoparticles effectively reduce chloride-induced compressive strength degradation in UHPFRC by refining the microstructure and limiting aggressive ion ingress, with an optimum performance observed at approximately 2.0 wt% LDH. These findings provide direct numerical evidence supporting the role of LDH in enhancing long-term mechanical stability under chloride-rich environments.

The enhancement in compressive strength observed in the presence

of LDH nanoparticles, particularly within a chloride environment, is fundamentally attributed to their unique physicochemical properties and their subsequent impact on the concrete's microstructure and chemistry. With their high ion-exchange capacity and lamellar structure, LDH nanoparticles effectively act as pore-refining agents, filling interstitial voids and reducing the overall porosity of the matrix. This densification directly contributes to a reduction in permeability, which in turn enhances the concrete's resistance to the ingress of chloride ions. Furthermore, LDH nanoparticles participate in the cement hydration process, acting as nucleation sites that promote the formation of additional hydration products, most notably Calcium Silicate Hydrate (C-S-H). This results in a strengthening of the microstructural bonds and an overall improvement in the intrinsic strength of the concrete. In a chloride environment, this reinforced structure physically impedes the penetration of chloride ions, thereby preserving compressive strength. This hypothesis is corroborated by the SEM analysis of the fracture surfaces, as presented in Fig. 6, which compares the normal UHPFRC specimen with those modified with 2.0 % and 2.5 % LDH nanoparticles. The SEM micrographs reveal a significant refinement of the microstructure in the LDH-modified UHPFRC. In the sample containing 2.0 % LDH, the nanoparticles are observed to be uniformly dispersed among the cement and aggregate particles, effectively filling the interstitial voids. This leads to reduced porosity and enhanced adhesion, creating a more densified and resilient concrete matrix. In contrast, the specimen with 2.5 % LDH exhibits evidence of increased porosity and areas of poor bonding between the cementitious phases and the nanoparticles, likely due to agglomeration. This compromised microstructure accounts for the observed reduction in compressive strength compared to the 2.0 % specimen. These microstructural observations confirm that LDH nanoparticles contribute to a refined and less permeable concrete matrix, which is the primary mechanism responsible for the enhanced performance, particularly in aggressive environments such as those with high chloride concentrations.

The reduction in compressive strength observed under chloride exposure, compared with normal curing conditions, arises from a combination of chloride-induced microstructural and physicochemical degradation mechanisms. Although UHPFRC is characterized by a highly dense and low-permeability matrix, prolonged exposure to chloride-rich environments can still induce localized deterioration, particularly in surface-near regions and microstructural weak zones. Chloride ingress may promote leaching of calcium-bearing hydration products and partial decalcification of the C–S–H gel, leading to reduced matrix cohesion and stiffness. In parallel, chloride ions interact with aluminate-containing hydration phases, resulting in phase transformations (e.g., AFm-to-Friedel's salt conversion) accompanied by local structural rearrangements and internal stress development. At the meso-scale, these chemically driven alterations are exacerbated by stress concentration effects within the interfacial transition zones (ITZs) surrounding steel microfibers, which exhibit comparatively higher porosity and compositional heterogeneity. Such regions facilitate microcrack initiation and gradual damage accumulation under chloride ingress and moisture fluctuations, thereby diminishing the effective load-bearing

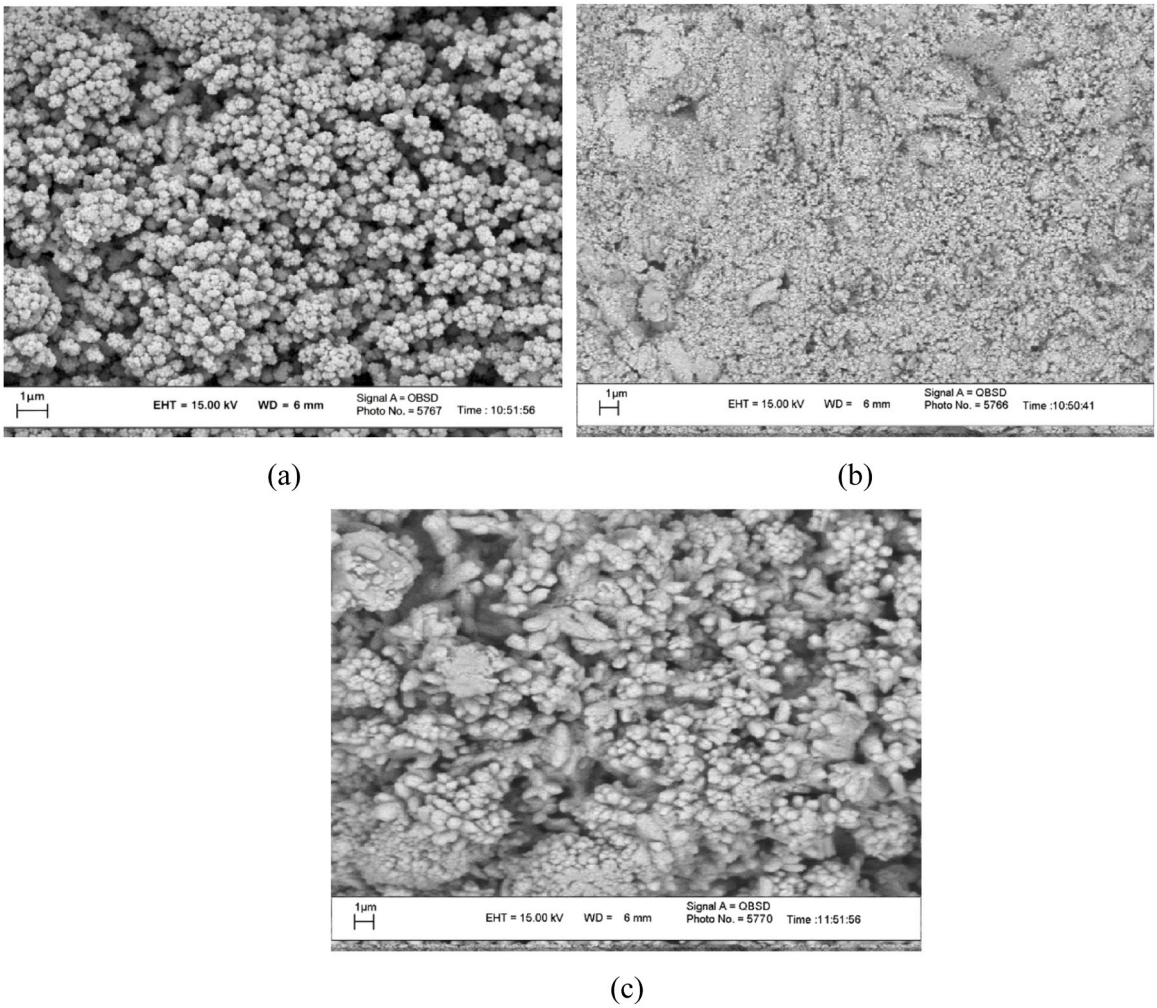


**Fig. 6.** Comparative SEM analysis of fracture surfaces showing the microstructure of: (a) plain UHPFRC (control), (b) UHPFRC with 2.0 % LDH nanoparticles, revealing a densified matrix, and (c) UHPFRC with 2.5 % LDH nanoparticles, showing increased porosity.

capacity of the matrix–fiber system. Collectively, the superposition of hydration-phase destabilization and microcrack development results in a measurable reduction in compressive strength under chloride exposure.

From a physicochemical standpoint, the reduction in compressive strength observed under chloride-exposed conditions can be attributed to a combination of chloride–hydration phase interactions and microstructural destabilization processes. Upon exposure to chloride-rich environments, free chloride ions ($Cl^-$) penetrate the cementitious matrix and interact primarily with aluminate-bearing hydration products. One of the dominant reactions involves the transformation of AFm phases into Friedel's salt, which can be expressed as:

$$AFm + 2Cl^- \rightarrow C_3A{\cdot}CaCl_2{\cdot}10H_2O \ \ (\text{Friedel's salt}) \tag{4}$$

Although the formation of Friedel's salt contributes to chemical chloride binding, this process is accompanied by local structural rearrangements and volumetric instability, which may induce micro-scale damage and reduce the effective stiffness of the load-bearing skeleton. In parallel, prolonged chloride exposure can promote leaching of portlandite:

$$Ca(OH)_2 \rightarrow Ca^{2+} + 2OH^- \tag{5}$$

The loss of calcium ions disrupts the chemical equilibrium of the calcium–silicate–hydrate (C–S–H) gel, leading to partial decalcification according to:

$$C-S-H \rightarrow C-S-H_{(Ca0poor)} + Ca^{2+} \tag{6}$$

This decalcification reduces the intrinsic stiffness and cohesion of the C–S–H network, thereby contributing to the observed compressive strength degradation, even in the highly compact matrix of UHPFRC.

The incorporation of LDH nanoparticles effectively mitigates these degradation mechanisms through their layered structure and anion-exchange capability. LDHs can capture free chloride ions via reversible anion substitution reactions:

$$LDH-OH + Cl^- \rightleftharpoons LDH-Cl + OH^- \tag{7}$$

This mechanism reduces the concentration of free chlorides in the pore solution, thereby limiting Friedel's salt formation and suppressing chloride-induced decalcification of C–S–H. Consequently, mixtures containing optimized LDH contents exhibit reduced compressive strength loss under chloride exposure. However, when the LDH dosage exceeds the optimal level (e.g., 2.5 wt% in the present study), nanoparticle agglomeration becomes more pronounced, reducing the effective reactive surface area available for chloride binding. These agglomerates act as local microstructural heterogeneities and weak zones, diminishing the chemical and microstructural protective role of LDH and leading to an increased strength reduction under chloride exposure. This transition from a chloride-mitigating regime to an agglomeration-dominated regime confirms the existence of an optimum LDH dosage for maximizing long-term mechanical stability in chloride-rich environments.

### 3.2. RCMT and Corrosion Resistance

A visual inspection of the specimen surfaces following the RCMT, as presented in Fig. 7, provides initial qualitative evidence of the LDH nanoparticles' efficacy. The figure compares the surface condition of the control UHPFRC specimen with that of the UHPFRC modified with 2.0 % LDH. A significant reduction in chloride-induced surface deterioration is apparent in the LDH-modified specimen, which exhibits a more intact and stable surface. In stark contrast, the control specimen shows clear signs of corrosion, with visible rust stains indicating the oxidation of the near-surface steel fibers.

Additional evidence supporting the durability enhancement is obtained from the examination of fracture surfaces after chloride exposure, as presented in Fig. 8. The cross-sectional images compare the reference UHPFRC specimen with those incorporating 1.0 wt% and 2.0 wt% LDH nanoparticles, enabling direct evaluation of internal damage characteristics. The control specimen displays more pronounced signs of internal deterioration, whereas the LDH-modified mixtures exhibit a noticeably more intact and homogeneous internal structure. In particular, the specimen containing 2.0 wt% LDH shows minimal internal degradation, indicating an improved resistance to chloride-induced damage. These observations qualitatively confirm the beneficial role of LDH nanoparticles in restricting chloride ingress and suppressing corrosion-related deterioration within the concrete matrix. The enhanced performance can be attributed to the microstructural refinement induced by LDH incorporation, which leads to reduced pore connectivity and lower permeability. As a result, the transport of aggressive ions is physically hindered, and the integrity of the cementitious matrix is better preserved. Consequently, LDH nanoparticles contribute to strengthening the internal structure of UHPFRC and significantly improving its durability when exposed to corrosive environments.

The chloride migration coefficients obtained from the RCMT at curing ages of 28 and 90 days are summarized in Table 4. As shown in Table 4, the control UHPFRC mixture exhibits the highest chloride migration coefficients at both ages, indicating a comparatively higher susceptibility to chloride ion transport despite the intrinsically dense UHPFRC matrix. With the incorporation of LDH nanoparticles, a systematic reduction in the CMC is observed for both curing periods, confirming the effectiveness of LDH in enhancing chloride resistance. From a quantitative perspective, at 28 days, the chloride migration coefficient

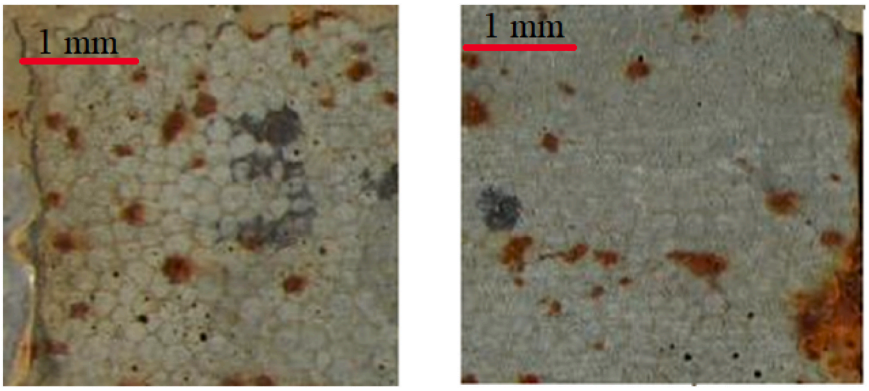


**Fig. 7.** Optical micrographs of UHPFRC surfaces after chloride exposure: (a) control specimen showing localized corrosion products and microcrack-affected zones; (b) LDH-modified specimen exhibiting a more uniform matrix with reduced corrosion features. Scale bars are included for reference.

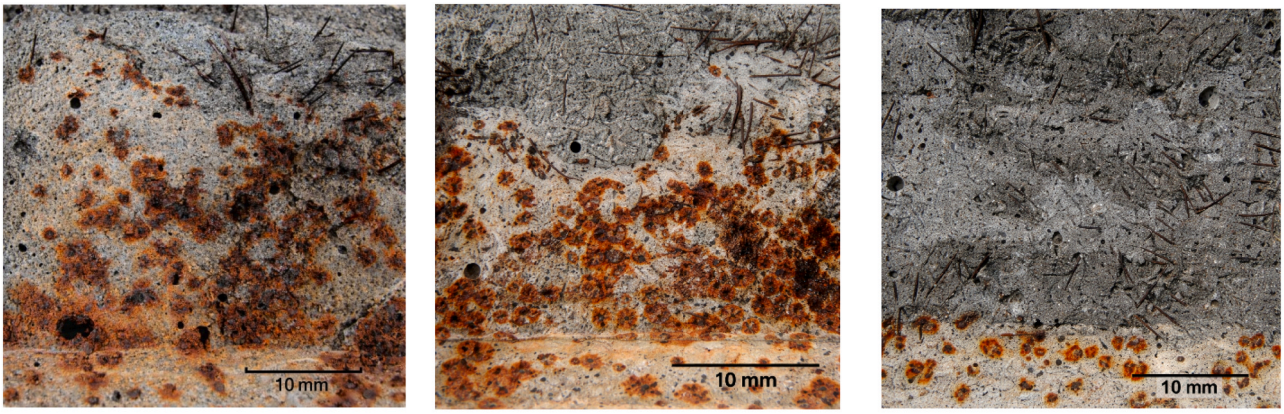


**Fig. 8.** Fracture surface morphologies of UHPFRC after chloride exposure: (a) control mixture; (b) 1.0 wt% LDH-modified UHPFRC; and (c) 2.0 wt% LDH-modified UHPFRC.

**Table 4**
Chloride migration coefficient (CMC) of LDH reinforced-UHPFRC mixtures at 28 and 90 days (RCMT).

| LDH content (wt%) | 28 days | | 90 days | |
|---|---|---|---|---|
| | CMC ($\times10^{-12}$ $m^2$/s) | Reduction vs. control (%) | CMC ($\times10^{-12}$ $m^2$/s) | Reduction vs. control (%) |
| 0.0 (Control) | 7.20 | – | 6.20 | – |
| 0.5 | 6.30 | 12.5 | 5.40 | 12.9 |
| 1.0 | 5.60 | 22.2 | 4.60 | 25.8 |
| 1.5 | 5.10 | 29.2 | 4.10 | 33.9 |
| 2.0 | 4.90 | 31.9 | 3.89 | 37.2 |
| 2.5 | 5.40 | 25.0 | 4.45 | 28.2 |

decreases progressively with increasing LDH content up to 2.0 wt%, where a maximum reduction of approximately 31.9 % relative to the control mixture is achieved (Table 4). At 90 days, this improvement becomes more pronounced, with the 2.0 wt% LDH mixture exhibiting a 37.2 % reduction in CMC compared to the control. The additional decrease in CMC at 90 days reflects the combined effects of continued cement hydration, further pore refinement, and enhanced chloride-binding capacity of LDH-modified matrices over time.

The physical interpretation of these trends is closely related to microstructural evolution. At moderate LDH dosages (≤2.0 wt%), well-dispersed LDH nanoparticles act as effective micro-fillers and hydration nucleation sites, leading to reduced capillary pore connectivity, increased diffusion tortuosity, and partial immobilization of free chloride ions through ion-exchange mechanisms. These effects collectively suppress chloride transport, resulting in lower migration coefficients. In contrast, the mixture containing 2.5 wt% LDH shows a partial rebound in CMC at both curing ages (Table 4). This behavior is attributed to nanoparticle agglomeration at excessive dosages, which induces local heterogeneities and inter-agglomerate voids that facilitate preferential chloride migration pathways. Nevertheless, even at 2.5 wt% LDH, the migration coefficients remain significantly lower than those of the control mixture, indicating an overall beneficial effect of LDH incorporation.

Overall, the results presented in Table 4 demonstrate that LDH nanoparticles substantially enhance the chloride resistance of UHPFRC, with 2.0 wt% LDH identified as the optimal dosage for minimizing chloride migration. The observed consistency between RCMT results and the trends obtained from capillary water absorption and sorptivity analyses further validates the role of LDH-induced pore refinement and transport pathway disruption in improving the durability performance of UHPFRC.

Furthermore, the data presented in Table 4 reveal a clear trend of decreasing chloride migration coefficients with increasing specimen age. This phenomenon is a direct consequence of the ongoing cement hydration process. In the early stages, as the concrete is curing, the hydration reactions are still progressing. Over time, as the concrete matures, these reactions proceed to a more advanced degree, leading to the formation of a greater volume of hydration products and the establishment of stronger chemical bonds between the cementitious phases and the aggregates. This process inherently results in a refinement of the pore structure and a densification of the concrete matrix. Consequently, at later ages, the chloride migration coefficient naturally decreases as the concrete becomes progressively more impermeable and resistant to ion penetration. While the initial contribution of the LDH nanoparticles may be less pronounced at very early ages, their beneficial effects—namely the pozzolanic reaction and the physical filler effect—become increasingly significant as the matrix matures. Over time, the synergistic interaction between the hydrating cement particles and the LDH nanoparticles leads to the formation of a more compact and tortuous microstructure. These microstructural developments are directly responsible for the reduction in porosity and the corresponding improvement in the concrete's resistance to chloride ion attack. Therefore, the observed decrease in the chloride migration coefficient at later ages is an expected outcome, reflecting the natural evolution and enhancement of the concrete's durability characteristics over time.

### 3.3. Capillary water absorption

Fig. 9 shows the cumulative capillary water absorption of LDH-modified UHPFRC mixtures in accordance with ASTM C1585. Cumulative capillary water absorption expressed in kg/$m^2$ as a function of the square root of time, in accordance with ASTM C1585. The progressive reduction in absorption and sorptivity up to 2.0 wt% LDH reflects effective pore refinement and reduced capillary connectivity, as confirmed by MIP analysis. The increased absorption at 2.5 wt% LDH is attributed to nanoparticle agglomeration and inter-agglomerate voids. A clear non-linear uptake behavior is observed: an initially faster absorption stage followed by a progressively reduced rate, which is typical for capillary suction where the driving capillary pressure remains but the hydraulic pathway becomes increasingly saturated and flow resistance rises with time. Across all time points, LDH-modified mixtures exhibit lower cumulative uptake than the control, indicating that LDH reduces capillary transport by modifying the pore network rather than merely delaying wetting.

From a quantitative standpoint, the control mixture reaches the highest cumulative absorption at the end of the monitoring period, while

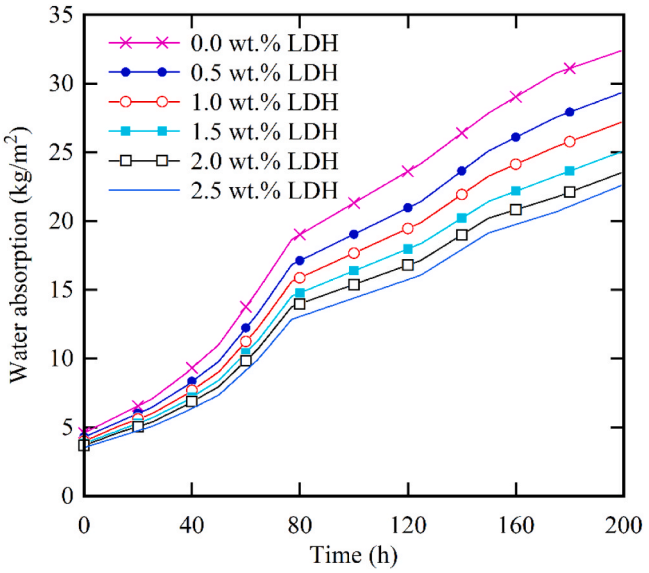


**Fig. 9.** Cumulative capillary water absorption profiles of UHPFRC mixtures with varying LDH nanoparticle contents over an 8-day exposure period, illustrating the influence of LDH dosage on capillary transport behavior relative to the control mixture.

LDH incorporation leads to a systematic reduction up to an optimum dosage of 2.0 wt%. Using the end-point values as an illustrative metric, the 2.0 wt% LDH mixture achieves the lowest cumulative uptake (≈ 27 % lower than the control at the final time), confirming superior resistance to water ingress. Intermediate dosages (0.5–1.5 wt%) show a progressive reduction relative to the control, demonstrating a dose-dependent improvement. Importantly, the 2.5 wt% LDH mixture exhibits a rebound (higher uptake than 2.0 wt%) yet remains lower than the control (≈ 30 % lower than the control at the final time), revealing a non-monotonic response at excessive LDH content. In addition to end-point comparison, the early-age absorption rate (sorptivity) follows the same trend: sorptivity decreases continuously from the control to 2.0 wt% and then increases at 2.5 wt%, consistent with an "optimum dosage" phenomenon for nanoparticle-modified cementitious matrices.

The physical interpretation is directly linked to pore structure evolution. At dosages up to 2.0 wt%, well-dispersed LDH platelets act as micro-fillers and hydration nucleation sites, which refine capillary pores, reduce pore connectivity, and increase diffusion tortuosity; consequently, both cumulative uptake and early-stage transport rate decrease. At 2.5 wt%, however, the high surface energy of LDH increases the tendency for agglomeration, producing inter-agglomerate voids and local heterogeneity. These features partially restore preferential capillary pathways, leading to the observed increase in absorption relative to the 2.0 wt% mixture. Overall, Fig. 9 provides consistent qualitative and quantitative evidence that LDH improves the moisture-transport resistance of UHPFRC, with an optimal performance near 2.0 wt%, while overdosage can compromise pore refinement efficiency due to dispersion limitations.

In this study, sorptivity was determined in accordance with ASTM C1585, which provides a standardized methodology for assessing water absorption and capillary suction characteristics of concrete. As summarized in Table 5, the sorptivity values of the UHPFRC mixtures exhibit a clear dependence on the LDH nanoparticle content. The control mixture shows the highest sorptivity, indicating a relatively continuous capillary pore network that facilitates rapid early-age water uptake. With increasing LDH content up to 2.0 wt%, sorptivity decreases progressively, reaching a minimum at 2.0 wt% LDH. Quantitatively, the sorptivity at this optimal dosage is reduced by approximately 25–30 % compared with the control specimen (Table 5), reflecting a significant suppression of early-stage capillary suction. Intermediate LDH dosages

**Table 5**
Sorptivity values of UHPFRC mixtures with varying LDH contents determined in accordance with ASTM C1585.

| LDH (wt%) | Sorptivity (S) ($kg.m^{-2}.s^{-1/2}$) |
|---|---|
| 0.0 | 0.0158 |
| 0.5 | 0.0142 |
| 1.0 | 0.0132 |
| 1.5 | 0.0124 |
| 2.0 | 0.0118 |
| 2.5 | 0.0126 |

(0.5–1.5 wt%) exhibit a gradual decline in sorptivity, confirming a dose-dependent improvement in resistance to capillary transport. In contrast, the mixture containing 2.5 wt% LDH shows an increase in sorptivity relative to the optimal mixture, although it remains lower than that of the control. This rebound behavior suggests a partial loss of pore refinement efficiency at excessive LDH content, which is consistent with dispersion-related effects such as nanoparticle agglomeration and the formation of inter-agglomerate voids. Overall, the sorptivity results obtained following ASTM C1585 provide quantitative support for the cumulative capillary absorption trends (Fig. 9) and are in good agreement with the pore structure evolution inferred from MIP analysis, confirming 2.0 wt% LDH as the optimal dosage for minimizing capillary water ingress in UHPFRC.

### 3.4. Pore structure characteristics based on MIP results

The pore structure parameters derived from MIP, as summarized in Table 6, clearly demonstrate the significant influence of LDH nanoparticle content on the microstructural characteristics of UHPFRC. The control mixture exhibits a relatively higher total porosity and larger critical pore diameter, accompanied by a considerable proportion of pores exceeding 100 nm, which are known to govern capillary transport and water absorption. With increasing LDH content up to 2.0 wt%, a systematic refinement of the pore structure is observed. This refinement is reflected by a continuous reduction in total porosity and pore volume, a decrease in both mean and critical pore diameters, and a progressive shift in pore size distribution toward finer pores (<20 nm and 20–60 nm). Concurrently, the pore specific surface area increases, indicating the formation of a denser and more complex pore network. Such trends are characteristic of nano-modified cementitious systems, where well-dispersed nanoparticles act as micro-fillers and hydration nucleation sites, thereby reducing capillary pore connectivity and increasing diffusion tortuosity, as widely reported in previous studies on UHPFRC and nanomodified concretes. Similar pore refinement trends identified by MIP have been widely reported for UHPFRC systems incorporating fine mineral additions, where micro-filler effects and enhanced hydration kinetics lead to reduced capillary pore connectivity and improved transport resistance [60].

In contrast, the mixture containing 2.5 wt% LDH shows a reversal of these beneficial trends. Although the LDH content is higher, both the total porosity and critical pore diameter increase compared with the optimal 2.0 wt% mixture, accompanied by a higher fraction of pores larger than 100 nm and a reduction in pore specific surface area. This behavior indicates a transition from a pore-refinement-dominated regime to an agglomeration-controlled microstructure, where excessive LDH promotes particle clustering and the formation of inter-agglomerate voids. These microstructural heterogeneities locally enhance capillary pore connectivity, providing preferential pathways for fluid transport. The observed MIP trends are therefore fully consistent with the measured increase in capillary water absorption and the reduced durability performance at 2.5 wt% LDH. This agglomeration-controlled pore structure evolution at higher nanoparticle contents is consistent with MIP-based observations reported for nano-modified cementitious systems, where excessive nanoparticle addition leads to particle clustering, increased critical pore diameter, and a resurgence of

**Table 6**
Pore structure characteristics of UHPFRC incorporating different LDH contents derived from MIP analysis.

| LDH (wt %) | Porosity (%) | Pore volume (cc/g) | Pore specific surface ($m^2$/g) | Mean pore diameter (nm) | Critical pore diameter (nm) | Pore proportions (%) by diameter (nm) | | | |
|---|---|---|---|---|---|---|---|---|---|
| | | | | | | < 20 | 20–60 | 60–100 | > 100 |
| 0.0 | 6.2 | 0.030 | 16.0 | 32 | 95 | 22 | 30 | 16 | 32 |
| 0.5 | 5.6 | 0.027 | 17.5 | 28 | 80 | 26 | 32 | 16 | 26 |
| 1.0 | 5.0 | 0.024 | 19.0 | 24 | 68 | 30 | 33 | 15 | 22 |
| 1.5 | 4.6 | 0.022 | 20.5 | 22 | 60 | 33 | 34 | 14 | 19 |
| 2.0 | 4.1 | 0.020 | 22.0 | 20 | 52 | 36 | 35 | 13 | 16 |
| 2.5 | 5.4 | 0.026 | 18.0 | 27 | 88 | 25 | 31 | 15 | 29 |

capillary-scale porosity despite an overall dense matrix [61]. Similar non-monotonic pore structure evolution at high nanoparticle dosages has been reported in the literature for nano-modified UHPFRC and cementitious composites, where optimal nanoparticle contents yield maximum microstructural densification, while overdosage leads to dispersion-related deterioration [62]. Overall, the MIP results confirm that 2.0 wt% LDH represents an optimal dosage for achieving pore refinement and improved transport resistance in UHPFRC. These MIP-derived trends provide microstructural evidence supporting the observed variations in capillary water absorption and compressive strength.

## 4. Conclusions

This study addressed the unresolved question of whether biodegradable LDH nanoparticles can systematically improve the compressive performance and chloride-related durability/transport resistance of UHPFRC when a constant dosage of steel microfibers is used for crack control. A comprehensive experimental program (compressive strength, ASTM C1585 capillary absorption/sorptivity, MIP pore structure, and RCMT/NT BUILD 492 chloride migration) was conducted for LDH dosages of 0–2.5 wt%. Overall, the results confirm a clear dose-dependent improvement up to an optimum, followed by performance loss at excessive dosage due to dispersion limitations. On the basis of the obtained results, the main conclusions of this study are summarized as follows:

- Compressive strength (28 days, normal curing): the control mixture reached 148.5 MPa, while the optimum mixture (2.0 wt% LDH) reached 182.67 MPa, i.e., + 21.95 % relative to control.
- Strength stability under chloride exposure (90 days): the control mixture exhibited ~14.1 % reduction relative to its 90-day normal-cured counterpart, whereas the 2.0 wt% LDH mixture limited the reduction to ~2.6 %, demonstrating strong mitigation of chloride-related degradation.
- Chloride migration coefficient (RCMT/NT BUILD 492): relative to control, the 2.0 wt% LDH mixture reduced CMC by 31.9 % at 28 days (7.20 → 4.90 $\times 10^{-12}$ $m^2/s$) and by 37.2 % at 90 days (6.20 → 3.89 $\times 10^{-12}$ $m^2/s$).
- Capillary absorption and sorptivity (ASTM C1585): sorptivity decreased from 0.0158 (control) to 0.0118 $kg \cdot m^{-2} \cdot s^{-1/2}$ at 2.0 wt% LDH (≈ 25 % reduction), indicating reduced capillary connectivity and moisture transport rate.
- Pore structure refinement (MIP evidence): at 2.0 wt% LDH, total porosity decreased from 6.2 % to 4.1 %, and the critical pore diameter decreased from 95 to 52 nm, consistent with a shift toward finer pores and reduced connected capillary pathways.

Mechanistic interpretation (why the optimum occurs)

At moderate LDH contents (≤2.0 wt%), the nanoparticles act as (i) micro-fillers and (ii) hydration nucleation sites, promoting matrix densification, reducing pore connectivity, increasing tortuosity, and providing additional chloride-binding/anion-exchange capacity. In parallel, the steel microfibers primarily restrict microcrack formation and propagation, limiting preferential transport channels. The combined action therefore produces a synergistic, multi-scale improvement in both mechanical capacity and transport resistance.

At 2.5 wt% LDH, performance partially deteriorates (higher sorptivity/absorption, larger critical pore diameter, and reduced strength gain) because the very low w/b UHPFRC matrix increases the tendency of LDH to agglomerate, creating local heterogeneity and inter-agglomerate voids that re-enable connected capillary paths and reduce the effective reactive surface area.

The findings are specific to the investigated constituents (binder system, w/b, LDH type/dispersion protocol, and fixed microfiber content). Future studies should (i) quantify long-term field exposure performance, (ii) examine broader LDH chemistries and dispersion strategies, and (iii) assess coupled mechanical–durability behavior under sustained loading and cyclic wet–dry chloride regimes.

## CRediT authorship contribution statement

**Volkan Gönen:** Writing – review & editing, Supervision, Data curation. **Hakan Çağlar:** Methodology, Investigation, Formal analysis. **Selcuk Çimen:** Writing – original draft, Methodology, Data curation. **Arzu Çağlar:** Writing – original draft, Methodology.

## Declaration of Competing Interest

The authors declare that there are no conflicts of interest related to the publication of this article.

## Data availability

Data will be made available on request.

## References

[1] I. Sharifi, M.H. Sherzai, A. Javanmard, F. Yalçındağ, İ.Ö. Yaman, Uniaxial tensile performance in the warp and weft directions of carbon textile reinforced concretes with two different matrices, Constr. Build. Mater. 476 (2025) 141292.
[2] J. Esmaeili, I. Sharifi, K. Andalibi, J. Kasaei, Effect of different matrix compositions and micro steel fibers on tensile behavior of textile reinforced concrete, in: In: IOP Conference Series: Materials Science and Engineering, 246, IOP Publishing, 2017 012031.
[3] J. Esmaeili, I. Sharifi, J. Kasaei, M. Nourizadeh, A. Ebrahimi Emamieh, Experimental and analytical investigation on strengthening of heat damaged concrete by textile reinforced concrete (TRC), Arch. Civ. Mech. Eng. 19 (2019) 1468–1483.
[4] I. Sharifi, An experimental investigation on uniaxial tensile, slip-bond. and creep behavior of carbon textile reinforced cementitious composites (C-TRCC) [dissertation]. Ankara (Turkey, Middle East Technical University, 2025.
[5] M. Pouraminian, A.E. Akbari Baghal, K. Andalibi, F. Khosravi, V. Arab Maleki, Enhancing the pull-out behavior of ribbed steel bars in CNT-modified UHPFRC using recycled steel fibers from waste tires: a multiscale finite element study, Sci. Rep. 14 (1) (2024) 19939.
[6] S. Regalla, N. Senthil Kumar, Experimental investigations on performance efficiency characteristics of ultra-high-performance concrete (UHPC) with enhanced sustainable mineral admixtures, J. Struct. Integr. Maint. 10 (3) (2025) 2538978.

[7] G. Wu, K. Yang, H. Zhang, Y. Hu, J. Qi, C. Lu, et al., Flexural performance of cracked UHPC under the coupled actions of sustained loading and corrosive environments, J. Mater. Civ. Eng. 37 (12) (2025) 04025467.
[8] S. Moghtadernejad, R. Bhadra, Z. Lounis, J. Zhang, Effects of climate change and environmental aggressiveness on onset of corrosion in concrete highway bridge decks, Struct. Infrastruct. Eng. 21 (2025) 1–17.
[9] L.-S. Lv, J.-Y. Wang, R.-C. Xiao, M.-S. Fang, Y. Tan, Chloride ion transport properties in microcracked ultra-high performance concrete in the marine environment, Constr. Build. Mater. 291 (2021) 123310.
[10] N.M. Vaziri, S. Salehipour, Performance of lightweight alkali-activated slag concrete before and after exposure to elevated temperatures: mechanical properties and durability, J. Build. Eng. 112 (15) (2025) 113907.
[11] H. Huang, M. Huang, W. Zhang, S. Pospisil, T. Wu, Experimental investigation on rehabilitation of corroded RC columns with BSP and HPFL under combined loadings, J. Struct. Eng. 146 (8) (2020) 04020157.
[12] H. Huang, M. Li, Y. Yuan, H. Bai, Theoretical analysis on the lateral drift of precast concrete frame with replaceable artificial controllable plastic hinges, J. Build. Eng. 62 (2022) 105386.
[13] H. Huang, M. Li, W. Zhang, Y. Yuan, Seismic behavior of a friction-type artificial plastic hinge for the precast beam–column connection, Arch. Civ. Mech. Eng. 22 (4) (2022) 201.
[14] X. Long, H. Li, P.M. Iyela, S.-B. Kang, Predicting the bond stress–slip behavior of steel reinforcement in concrete under static and dynamic loadings by finite element, deep learning and analytical methods, Eng. Fail. Anal. 161 (2024) 108312.
[15] K. Qian, L. Cui, X. Deng, X. Zhang, Experimental and analytical study of BFRP bar reinforced UHPC beams under static and impact loading, Int. J. Impact Eng. 206 (2025) 105456.
[16] H. Yang, S. Li, J. Shu, H. Yu, H. Liu, Y. Xu, et al., Data-driven high-resolution total focus imaging from array ultrasonic time-domain signals of reinforced concrete material, Constr. Build. Mater. 492 (2025) 143048.
[17] W. Zhang, J. Lin, A fatigue-dependent cohesive zone model for SFRC-RC-CFRP composite beams: development and experimental validation, Structures 80 (2025) 109977.
[18] L. Sun, X. Wang, C. Zhang, Three-dimensional high fidelity mesoscale rapid modelling algorithm for concrete, Structures 70 (2024) 107561.
[19] D. Lu, F. Meng, X. Zhou, Y. Zhuo, Z. Gao, X. Du, A dynamic elastoplastic model of concrete based on a modeling method with environmental factors as constitutive variables, J. Eng. Mech. 149 (12) (2023) 04023102.
[20] D. Lu, G. Wang, X. Du, Y. Wang, A nonlinear dynamic uniaxial strength criterion that considers the ultimate dynamic strength of concrete, Int. J. Impact Eng. 103 (2017) 124–137.
[21] X. Zhou, A. Shi, D. Lu, Y. Chen, X. Zhuang, X. Lu, et al., A return mapping algorithm based on the hyper dual step derivative approximation for elastoplastic models, Comput. Methods Appl. Mech. Eng. 417 (2023) 116418.
[22] X. Zhou, D. Lu, J. Zhao, Y. Zhang, Z. Gao, T. Rabczuk, et al., Material characteristic length insensitive nonlocal modelling: a computationally efficient scaled nonlocal integral method, Comput. Geotech. 188 (2025) 107587.
[23] Y. Guo, S. Chen, M.T. Lakhiar, S. Zhuang, I.W. Lakhiar, Ternary binders and recycled turbine blade fibres in mortar: reducing embodied carbon in coastal construction, Constr. Build. Mater. 501 (2025) 144277.
[24] Y. Song, X. Diao, R. Xu, X. Wang, Y. Han, T. Shi, et al., A comprehensive review of mineral carbonation of civil engineering materials: a bibliometric analysis, Environ. Sci. Technol. 59 (2025) 26917–26944.
[25] M. Malekzadeh, M. Shishesaz, R. Mosalmani, V.A. Maleki, A. Yaghootian, Carbon nanotube reinforced 3D printed PMMA filaments: mechanical enhancement through experimental and multi-scale modeling, Mater. Chem. Phys. 345 (2025) 131194.
[26] D. Fayazi, A. Dolatimehr, A. Teymoori, S. Khalili, N.M. Vaziri, Z. Khaksar, Uniform dispersion of Bi2Sn2O7 nanoparticles on intersectional CuO monolayers for levofloxacin photodegradation: exploring influence of morphology on S-type charge migration, J. Water Process Eng. 77 (2025) 108626.
[27] Y. Yu, G. Zhu, Q. Zhang, M. Behzadnia, Z. Yang, Y. Liu, et al., Multinonmetal-doped V2O5 nanocomposites for lithium-ion battery cathodes, ACS Appl. Energy Mater. 7 (23) (2024) 11031–11037.
[28] M. Pirani, M. Hahn, H.D. Joghan, A.E. Tekkaya, S. Farahani, On the potential of manufacturing multi-material components with micro/nanocellular structures via the hybrid process of electromagnetic forming injection foaming, J. Micro Nano Sci. Eng. 12 (3) (2024) 031001.
[29] Y. Fazeli, Z. Nourbakhsh, S. Yalameha, D. Vashaee, Anisotropic elasticity, spin–orbit coupling, and topological properties of ZrTe2 and NiTe2: a comparative study for spintronic and nanoscale applications, Nanomaterials 15 (2) (2025) 148.
[30] J. Bao, J. Wei, P. Zhang, Z. Zhuang, T. Zhao, Experimental and theoretical investigation of chloride ingress into concrete exposed to real marine environment, Cem. Concr. Compos. 130 (2022) 104511.
[31] N. Saladi, L. Montanari, I. De la Varga, R. Spragg, B. Graybeal, Assessing durability properties of ultra-high performance concrete-class materials, Mater. Struct. 56 (8) (2023) 155.
[32] S. Saleh, A.H. Mahmood, E. Hamed, X.-L. Zhao, The mechanical, transport and chloride binding characteristics of ultra-high-performance concrete utilising seawater, sea sand and SCMs, Constr. Build. Mater. 372 (2023) 130815.
[33] S. Li, Y. Jiang, J. Zhou, Fracture resistance of UHPC-CA with amorphous silica: competition between microstructure densification and shrinkage microcracking, Theor. Appl. Fract. Mech. 138 (2025) 104886.
[34] S. Li, O.M. Jensen, Q. Yu, Enhancing the rate-dependent cracking resistance of UHPC under mixed tensile-shear mode by calcined bauxite aggregate, Cem. Concr. Compos. 159 (2025) 105993.
[35] C. Gu, G. Ye, Q. Wang, W. Sun, Modeling of the chloride diffusivity of ultra-high performance concrete with a multi-scale scheme, Model. Simul. Mater. Sci. Eng. 27 (5) (2019) 055002.
[36] K. Ojaghi, F. Kalateh, M.A.L. Lotfollahi Yaghin, Review on the impact of nanoparticle additives on fiber adhesion in ultra-high performance concrete for corrosive traffic environments, Int. J. Transp. Eng. 12 (4) (2025) 1947–1972.
[37] D. Hendrix, B.D. Huey, K. Wille, Nanosilica enhanced ultra-high performance concrete through hydrochloride acid or polyethylene glycol stabilization, Constr. Build. Mater. 425 (2024) 135977.
[38] L. Zhou, Y. Cai, C. Ma, Experimental study and numerical analysis of chloride ion diffusion in hydrotalcite concrete in chloride salt environment, Materials 16 (19) (2023) 6349.
[39] H. Chen, G. Zhang, Q. Ding, J. Zhu, J. Yang, J. Fu, et al., Effect of lightweight aggregate pre-wetting degree on the chloride ion permeability of ultra-high performance concrete, J. Build. Eng. 100 (2025) 111777.
[40] L. Zhang, H. Wang, A. Wang, Q. Zhang, Z. Li, X. Wang, et al., Experimental study of marine ultra-high-performance concrete with coarse aggregate (UHPC-CA), Case Stud. Constr. Mater. 22 (2025) e04731.
[41] L. Galli, P. Suraneni, Durability and damage resistance of sustainable Portland limestone cement-based (ultra) high-performance concrete in seawater, Mater. Struct. 58 (9) (2025) 310.
[42] M. Chen, H. Yuan, X. Qin, Y. Wang, H. Zheng, L. Yu, et al., Improve corrosion resistance of steel bars in simulated concrete pore solution by the addition of EDTA intercalated CaAl-LDH, Corros. Sci. 226 (2024) 111636.
[43] H. Yang, Y. Li, D. Zhang, R. Ding, C. Xiong, Study on corrosion protection of NA/LDH for reinforced concrete under dry-wet cycles conditions of NaCl solution, J. Build. Eng. 111 (2025) 113297.
[44] Y. Tian, Q. Li, C. Wen, N. Wang, Z. Zeng, LDH-inhibitor conversion film on steel rebar for mitigating chloride-induced corrosion in reinforced concrete environment, Constr. Build. Mater. 501 (2025) 144306.
[45] K. Cao, Z. Yan, K. Wang, S. Zhang, Y. Zhang, Q. Chen, et al., Mechanical properties, durability and microstructures of calcined layered double hydroxide mortar in marine environment, Case Stud. Constr. Mater. 23 (2025) e05091.
[46] P. Ramazani, T. Moradi Shaghaghi, M. Farzam, H. Afshin, M.A. Behnajady, Flexural strength of light-weight steel fiber reinforced concrete containing biodegradable LDHs microparticles: experimental study and multiscale finite element model, Int. J. Concr. Struct. Mater. 18 (1) (2024) 37.
[47] A. Mohsen, M.S. Amin, F.A. Selim, M. Ramadan, The impact of wurtzite and mesoporous Zn-Al-CO3 LDH on the performance of alkali-activated-slag: setting times, compressive strength, and radiation attenuation, Constr. Build. Mater. 438 (2024) 137218.
[48] Q. Yu, X. Ming, Y. Wang, L. Sun, M. Cui, G. Sun, Effects of highly dispersed LDH nano-platelets on chloride binding and corrosion protection of cementitious materials, Cem. Concr. Compos. 163 (2025) 106178.
[49] X. Pang, Y. Yuan, H. Liu, X. Pang, L. Chen, Y. Liu, et al., Highly dispersed and thermally stable PCE-LDH and its application as hardening accelerator for mortar, Constr. Build. Mater. 328 (2022) 127072.
[50] F. Kalateh, K. Ojaghi, M.A.L. Lotfollahi Yaghin, Experimental and numerical study on the pull-out behavior of steel fibers in ultra-high-strength concrete reinforced with biodegradable nanoparticles, Constr. Build. Mater. 500 (2025) 144171.
[51] Z. Qu, Q. Yu, H.J.H. Brouwers, Relationship between the particle size and dosage of LDHs and concrete resistance against chloride ingress, Cem. Concr. Res. 105 (2018) 81–90.
[52] F.Y. Al-Saffar, L.S. Wong, S.C. Paul, An elucidative review of the nanomaterial effect on the durability and calcium-silicate-hydrate (CSH) gel development of concrete, Gels 9 (8) (2023) 613.
[53] S.S. Hashemi, A. Ganjali, A. Mirzakhani, H. Irani, S. Dezhampanah, Effect of magnesium oxide and copper oxide nanoparticles on UHPC properties under different curing conditions, Constr. Build. Mater. 427 (2024) 136198.
[54] M. Chauhan, J.V. Dipak, G.B. Bhavin, Experimental investigation of ultra-high performance concrete using nano materials: a state of art review. In: AIP Conference Proceedings, AIP Publishing, 2024.
[55] D.-Y. Yoo, T. Oh, N. Banthia, Nanomaterials in ultra-high-performance concrete (UHPC) – a review, Cem. Concr. Compos. 134 (2022) 104730.
[56] S.A. Mostafa, M.M. El-Deeb, A.A. Farghali, A.S. Faried, Evaluation of the nano silica and nano waste materials on the corrosion protection of high strength steel embedded in ultra-high performance concrete, Sci. Rep. 11 (1) (2021) 2617.
[57] ASTM C1585-13, Standard test method for measurement of rate of absorption of water by hydraulic-cement concretes, ASTM International, West Conshohocken (PA), 2013.
[58] J. Wang, W. Dong, Water and chloride ion transport characteristics of unsaturated aeolian sand mortar under capillary absorption, J. Mater. Civ. Eng. 36 (9) (2024) 04024288.
[59] W.S. de Jesus, S.F.M. da Silva, T.M.S. de Almeida, M.T. Souza, E.S. Leal, R.S. Souza, et al., Comparative study of ASTM C1202 and IBRACON/NT Build 492 testing methods for assessing chloride ion penetration in concretes using different types of cement, Buildings 15 (3) (2025) 302.

[60] P. Spiesz, Q. Yu, H.J.H. Brouwers, Development of cement-based lightweight composites – Part 2: durability-related properties, Cem. Concr. Compos. 44 (2013) 30–40.

[61] J.J. Gaitero, I. Campillo, A. Guerrero, Reduction of the calcium leaching rate of cement paste by addition of silica nanoparticles, Cem. Concr. Res. 38 (8–9) (2008) 1112–1118.

[62] M.-H. Zhang, O.E. Gjørv, Microstructure of the interfacial zone between lightweight aggregate and cement paste, Cem. Concr. Res. 20 (4) (1990) 610–618.